ARTICLE

Distance Dependent Energy Transfer Dynamics from Molecular Donor to Zeolitic Imidazolate Framework Acceptor

_{ary 20xx,} Wenhui Hu,^a Fan Yang,^b Nick Pietraszak,^a Jing Gu,^{*b} Jier Huang^{*a}

Received 00th January 20xx, Accepted 00th January 20xx

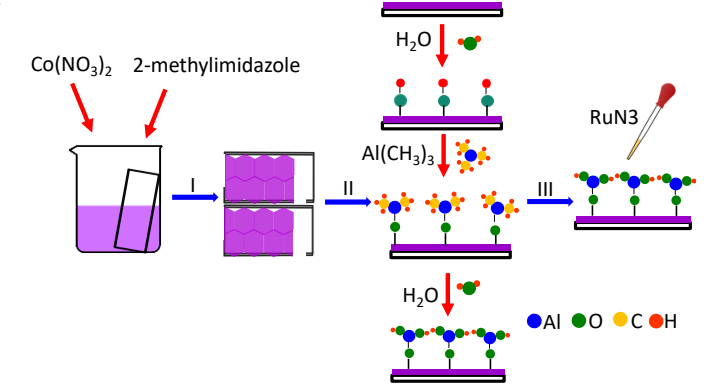
DOI: 10.1039/x0xx00000x

Zeolitic Imidazolate frameworks (ZIFs) have demonstrated as promising light harvesting and photocatalytic materials for solar energy conversion. To facilitate their application in photocatalysis, it is essential to develop a fundamental understanding on their light absorption property and energy transfer dynamics. In this work, we report distance-dependent energy transfer dynamics from a molecular photosensitizer (RuN3) to ZIF-67, where the distance between RuN3 and ZIF-67 is finely tuned by depositing ultrathin Al_2O_3 layer on ZIF-67 surface using atomic layer deposition (ALD) method. We show that energy transfer time decreases with increasing distance between RuN3 to ZIF-67 and the Förster radius is estimated to be 14.4 nm.

Introduction

Zeolitic imidazolate frameworks (ZIFs), a subclass of metal organic frameworks (MOFs), are composed of Zn²⁺ or Co²⁺ node tetrahedrally coordinated with imidazole-based organic linkers.¹⁻⁵ Owing to their ordered porous structure and large surface area, ZIFs have emerged as new materials for gas storage and separation, 6-9 chemical sensing, 10, 11 and catalysis. 12-¹⁴ Driven by the demand of renewable energy and environmental concerns, recent interests have extended their application in photocatalysis with a number of reports having demonstrated their capability as photocatalytic materials. 15-19 However, in majority of these systems, ZIFs were either used as hosts for reaction substrates/catalytic active species or templates to synthesize porous hybrid materials through annealing process.²⁰⁻²⁴ In contrast, our recent studies showed that ZIFs based on Co nodes and 2-methyl imidazolate ligand (ZIF-67) not only possess broad absorption in UV-visible-near IR region but also exhibit a long-lived excited state (ES), where the porous framework of ZIF-67 plays a central role in the formation of the long-lived ES.^{25, 26} A further study then showed that the electron in this ES state can be extracted through interfacial electron transfer (ET) from excited ZIF-67 to methylene blue, which largely demonstrates the promise of using ZIFs as intrinsic

While ZIF-67 has broad absorption in both visible and near IR region, the extinction coefficients of these spectral transitions resulting from dipole forbidden d-d transitions of Co nodes are quite low (~100-1000 mol·L-1·cm-1).28 In response to this challenge, we encapsulated molecular (RuN3)29 and semiconductor (CdS)30 photosensitizers (PS), which have absorption in visible region that compensates the absorption of ZIF-67 and have much larger extinction coefficient, into ZIF-67. We showed that both systems can strengthen the light harvesting ability of ZIF-67 as efficient energy transfer (ENT) can occur from guest PSs to ZIF-67. These results demonstrate that encapsulating a guest unit chromophore that can relay energy to ZIFs through ENT is a promising approach to enhance the light



Scheme 1. Schematic representation of the synthesis of RuN3/Al $_2O_3/ZIF$ -67 thin film.

light harvesting and charge separation materials for solar energy conversion.²⁷

^a-Department of Chemistry, Marquette University, Milwaukee, Wisconsin, 53201, USA.

b. Department of Chemistry and Biochemistry, San Diego State University, San Diego, California 92182, USA.

[†] Jier Huang (jier.huang@marquette.edu), Jing Gu (jgu@sdsu.edu). Electronic Supplementary Information (ESI) available: details of experimental methods, XRD, UV-Visible absorption spectra, transient absorption spectra. See DOI: 10.1039/x0xx00000x

ARTICLE Journal Name

harvesting ability of ZIFs. A natural question that follows these ENT studies is to unravel the key factors that control the dynamics of ENT. It has been shown previously that ENT efficiency is largely dependent on the distance between the donor and acceptor. $^{31-38}$ In this work, we report the impact of distance between RuN3 and ZIF-67 on the ENT dynamics in RuN3/ZIF-67 hybrid. The distance between RuN3 and ZIF-67 is controlled by tuning the thickness of the Al₂O₃ layer from 3 nm to 8.5 nm, which is deposited on the surface of ZIF-67 film before sensitization of RuN3 by atomic layer deposition (ALD). We show that the ENT efficiency decreases with the increasing thickness of Al₂O₃ between RuN3 and ZIF-67, where the theoretical Förster radius estimated according to the reported point to plane resonance energy transfer under 4th-power law $^{33, 39, 40}$ is 14.4 nm.

Results and discussion

The schematic representation of the synthesis of RuN3/Al₂O₃/ZIF-67 hybrid films is illustrated in scheme 1 (see details in supporting information). In the first step, a glass slide pre-treated with Piranha solution was immersed into the mixture of Co(NO₃)₂·6H₂O and 2-methylimidazole (2mIm). After about 1h, transparent and continuous ZIF-67 film was formed on both sides of the glass slide (step I).^{25, 29} ZIF-67 crystals on one side of the film is scratched off to make a single-side ZIF-67 film. Al₂O₃ layer with different thickness was then deposited on the surface of ZIF-67 film using ALD (step II). At temperature of 100-200°C, the deposition of Al₂O₃ usually has a stable growth rate of 0.1-0.11 nm/cycle on non-porous substrates.41-43 However, as demonstrated by the transmission electron microscopy (TEM) images, a much thicker layer of Al₂O₃ was identified (Figure S1). This can be explained by the nanoporous structure of ZIF-67, where Al₂O₃ is not only deposited on the surface but also the subsurface in the nanostructure. As a result, alternatively depositing 10 to 40 cycles of trimethylaluminum and water at 120°C resulted into 3 nm to 8.5 nm Al_2O_3 thin film on ZIF-67 (Table S1). After the deposition of Al₂O₃, the same amount of RuN3 in methanol solution was dropped onto the Al₂O₃/ZIF-67 films to form RuN3/Al₂O₃/ZIF-67 hybrid films (step III).

Figure 1a shows the XRD patterns of blank glass slides, Al_2O_3 on glass slides, ZIF-67 on glass slide, $Al_2O_3(8.5 \text{ nm})/\text{ZIF-67}$, and

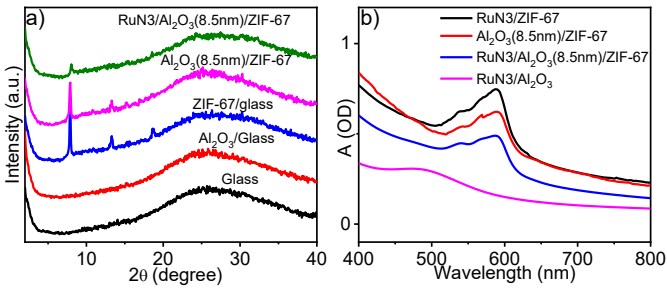


Figure 1. a) XRD patterns of glass, Al₂O₃/glass, ZIF-67/glass, Al₂O₃(8.5nm)/ZIF-67 and RuN3/Al₂O₃(8.5nm)/ZIF-67; b) UV-visible absorption spectra of RuN3/ZIF-67, Al₂O₃(8.5nm)/ZIF-67, RuN3/Al₂O₃ (8.5nm)/ZIF-67 and RuN3/Al₂O₃.

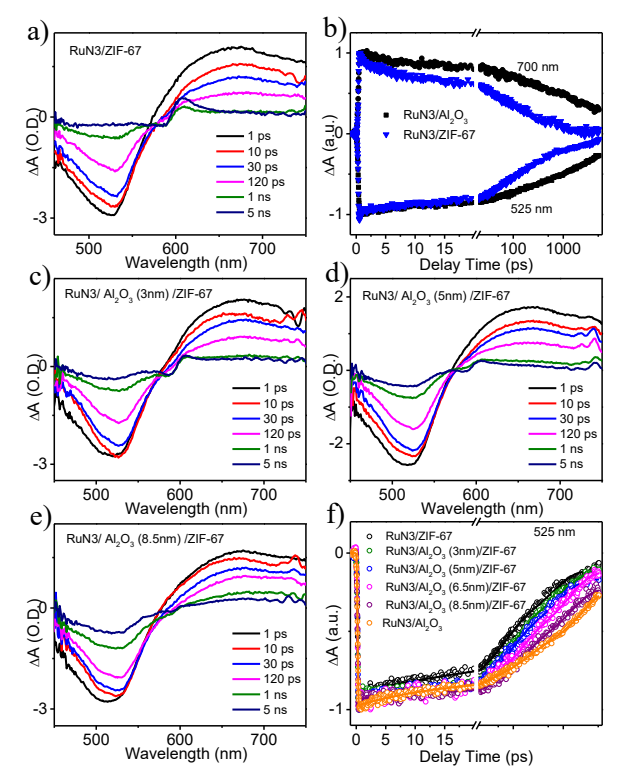


Figure 2. Transient absorption spectra of RuN3/ZIF-67 (a), RuN3/Al $_2$ O $_3$ (3nm)/ZIF-67 (c), RuN3/Al $_2$ O $_3$ (5nm)/ZIF-67 (d), and RuN3/Al $_2$ O $_3$ (8.5nm)/ZIF-67 (e); b) the comparison of GSB recovery and ESA decay kinetics of RuN3 on ZIF-67 and Al $_2$ O $_3$; f) The comparison of GSB recovery kinetics of RuN3 on different substrate.

RuN3/Al₂O₃(8.5 nm)/ZIF-67. A broad peak was observed in the range of 20° to 40° among all samples including the naked glass slide, which can be attributed to the diffraction of amorphous glass. Al₂O₃/ZIF-67 and RuN3/Al₂O₃/ZIF-67 films (Figure 1a, S2a, and S2b) all show similar XRD patterns to ZIF-67 film on glass, suggesting that ZIF-67 structure retains in the films after ALD deposition of Al₂O₃ and RuN3 sensitization. Note that the diffraction patterns of ZIF-67 film on glass seem different from that of ZIF-67 crystals (Figure S2). This can be attributed to the impact of glass slide on the diffraction patterns as the XRD patterns of ZIF-67 crystals scratched off from the glass slide resemble that of ZIF-67 crystals synthesized from the standard growth (Figure S2c). The retain of ZIF-67 structure in these hybrid films was further supported by the UV-Visible absorption spectra (Figure 1b and Figure S3), where Al₂O₃/ZIF-67 and RuN3/Al₂O₃/ZIF-67 films with different thickness of Al₂O₃ all show absorption peak centered at 585 nm originating from T_d Coll d-d transition, consistent with that of ZIF-67.25 While RuN3 has prominent absorption peak around 500 nm corresponding to ligand-to-metal charge transfer band (LMCT) (pink plot in Figure 1b), it cannot be easily seen from the UV-visible absorption spectrum of RuN3/ZIF-67 due to its overlap with ZIF-67 absorption. Nevertheless, the transient absorption experiments below confirm the adsorption of RuN3 on the surface of Al₂O₃/ZIF-67 film.

Journal Name ARTICLE

Transient absorption (TA) spectroscopy is used to examine the impact of the thickness of Al₂O₃ layer on the ENT dynamics from RuN3 to ZIF-67. Figure 2a shows the TA spectra of RuN3/ZIF-67 following 410 nm excitation which selectively excites RuN3 as ZIF-67 has negligible absorption at 410 nm. Consistent with previous literature result,²⁹ immediately following the excitation, the TA spectra of RuN3/ZIF-67 show a negative ground state bleach (GSB) centered at ~ 530 nm and a broad positive excited state absorption (ESA) feature at > 570 nm, which is due to the excitation of RuN3, resulting in the depopulation of RuN3 ground state and population of RuN3 excited state. As the lifetime of excited singlet state of LMCT ($^{1}LMCT$) is < 100 fs, $^{44, 45}$ which is much faster than our instrument response time (~ 200 fs), the ESA absorption of RuN3 can be attributed to ³LMCT. The GSB of RuN3 recovers and ESA decays with

Table 1. The half lifetime of RuN3 GSB on different films and estimated ENT time and efficiency of RuN3/Al $_2O_3/ZIF$ -67

	τ (ps)	τ (ps)	η (100%) ENT
RuN3/ZIF-67	96	106	90.6
RuN3/Al ₂ O ₃ (3nm)/ZIF-67	158	188	84.0
RuN3/Al ₂ O ₃ (5nm)/ZIF-67	182	223	81.6
RuN3/Al ₂ O ₃ (6.5nm)/ZIF-67	287	406	70.7
RuN3/Al ₂ O ₃ (8.5nm)/ZIF-67	528	1147	46.0
RuN3/Al ₂ O ₃ (τ_0)	978	-	-

time simultaneously (Figure 2b), which is accompanied by the formation of a derivative feature consisting of a negative feature centered at 585 nm and absorption at 605 nm at later time (> 200 ps), consistent with the typical spectral features of the excited state of ZIF-67 corresponding to ${}^4A_2(F)$ - ${}^4T_1(P)$ Co d-d transition, 17, 25 suggesting that the excitation of RuN3 leads to the formation of excited ZIF-67.²⁹ Moreover, the GSB recovery and ESA decay in RuN3/ZIF-67 are much faster than that of RuN3/Al₂O₃ (Figure 2b), where the latter is used as a model system for intrinsic ES dynamics of RuN3 on a solid surface as ENT from RuN3 to Al₂O₃ is not expected due to significantly larger band gap of Al₂O₃ than RuN3.⁴⁶⁻⁴⁸ These results together support that ENT occurs from RuN3 (3LMCT) to ZIF-67 (4A2) following the excitation of RuN3, which quenches the ES of RuN3 and results in the formation ZIF-67 ES, consistent with the previous report.²⁹ With the presence of Al₂O₃ layer (3 nm thickness) between RuN3 and ZIF-67 (Figure 2c), the TA spectra of RuN3/Al₂O₃(3 nm)/ZIF-67 resemble that of RuN3/ZIF-67. However, with increasing thickness of Al₂O₃, the derivative feature corresponding to ES of ZIF-67 in RuN3/Al₂O₃/ZIF-67 becomes weaker and weaker (Figure 2d-2e and Figure S4) and can be barely seen when the thickness of Al_2O_3 is 8.5 nm (Figure 2e). These results suggest that ENT process is partially blocked

by Al_2O_3 due to its inert nature, which results in decreasing ENT rate with increasing thickness of Al_2O_3 .

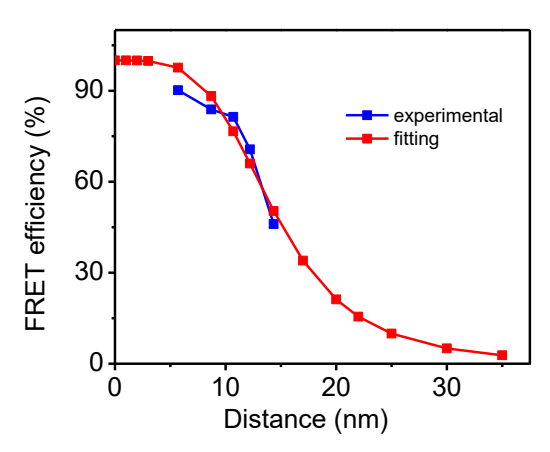


Figure 3. The ENT efficiency as a function of distance between ZIF-67 and RuN3.

The dependence of ENT process on Al₂O₃ thickness can be more clearly seen from the comparison of the GSB kinetics of RuN3 at 525 nm (Figure 2f) or ESA of RuN3 (Figure S5) among RuN3/Al₂O₃/ZIF-67 samples with different thickness of Al₂O₃. As shown in Figure 2f, the GSB recovery kinetics of RuN3/Al₂O₃/ZIF-67 becomes slower with the increasing thickness of Al_2O_3 , consistent with the assignment above. Since the recovery lifetime of GSB of these RuN3/Al₂O₃/ZIF-67 samples is much longer than 5 ns, which is beyond our TA time window, the ENT time was calculated based on the half lifetime $(\tau_{1/2})$, which is the time that the kinetic trace decays to half of its maximum amplitude. As listed in Table 1, $\tau_{1/2}$ for $RuN3/Al_2O_3/ZIF-67$ with 0 nm, 3 nm, 5 nm, 6.5 nm, and 8.5 nm is 96 ps, 158 ps, 182 ps, 287 ps, 528 ps, respectively. According to these half lifetimes, we estimated the ENT time according to equation 1.

$$1/\tau_{1/2} = 1/\tau_0 + 1/\tau_{ENT}$$
 (1)
 $\eta = \tau_{1/2}/\tau_{ENT}$ (2)

where τ_{ENT} is the ENT time from RuN3 to ZIF-67 and τ_0 is the intrinsic ES decay time of RuN3. ENT efficiency (η) can then be calculated according to equation 2. The calculated ENT efficiency is also listed in Table 1. The ENT efficiency decreased almost half (from 90.6% to 46.0%) when the thickness of Al $_2$ O $_3$ thin film increased to 8.5 nm, indicating that ENT efficiency in RuN3/ZIF-67 system is sensitive to the distance between RuN3 and ZIF-67.

The theoretical Förster radius of this system was estimated by fitting the experimental data using equation 3:^{33, 39, 40}

$$\eta = 1/[1+(R/R_0)^4]$$
 (3)

where R_0 and R are the Förster radius and distance between the donor and acceptor, respectively. R_0 equals to R when the ENT efficiency reaches 50%. In the fitting process, the distance between ZIF-67 and RuN3 without Al_2O_3 (r) and the Förster radius (R_0) were used as fitting parameters, where R is the sum of r and the thickness of Al_2O_3 layer. As shown in Figure 3, the experimental results can be adequately fit by the proposed model. From the best fitting, we obtained r value of 5.7 nm and R_0 of 14.4 nm. The R_0 value in this system is much higher than the previously reported molecular donor/acceptor system (< 5 nm). 29 , 49 , 50 Given that larger R_0 value results in higher FRET

ARTICLE Journal Name

efficiency (equation 3), $^{50, 51}$ the much higher value in current RuN3/ZIF-67 than the molecular systems suggests that the framework of ZIF might be beneficial for ENT process. In addition, a larger R_0 value can typically facilitate long-range energy transfer, 52 which suggests the potential of further enhancing the light absorption ability of ZIF systems through controlling ENT process.

Conclusion

In summary, we report the ENT dynamics from RuN3 to ZIF-67 and the impact of distance between RuN3 (donor) and ZIF-67 (acceptor) on ENT efficiency, where the distance between donor and acceptor was controlled by tuning the thickness of Al₂O₃ film deposited on the surface of ZIF-67 using atomic layer deposition (ALD). Using transient absorption spectroscopy, we show that ENT efficiency decreases with increasing thickness of the Al₂O₃ layer between RuN3 and ZIF-67. According to these experimental results, the Förster radius for this system was estimated to be 14.4 nm, which is much larger than many molecular donor/acceptor systems, suggesting the promise of enhancing light harvesting capability of ZIFs through ENT process. This work not only demonstrates the capability to tuning the distance of donor and acceptor by depositing different-thickness Al₂O₃ layers using ALD but also provides new insight on controlling ENT dynamics in RuN3/ZIF-67.

Conflicts of interest

There are no conflicts to declare

Author Contributions

The manuscript was written through contributions of all authors. All authors have given approval to the final version of the manuscript.

Acknowledgements

This work was supported by National Science Foundation (DMR-1654140) and ACS-PRF (57503-DNI6). Wenhui Hu acknowledge the John J. Eisch fellowship during the 2019-2020 academic year.

Notes and references

- 1. R. Banerjee, A. Phan, B. Wang, C. Knobler, H. Furukawa, M. O'Keeffe and O. M. Yaghi, Science **319** (5865), 939-943 (2008).
- 2. Y. Q. Tian, Z. X. Chen, L. H. Weng, H. B. Guo, S. Gao and D. Y. Zhao, Inorg. Chem. **43** (15), 4631-4635 (2004).
- 3. H. Hayashi, A. P. Cote, H. Furukawa, M. O'Keeffe and O. M. Yaghi, Nat. Mater. **6** (7), 501-506 (2007).
- S. R. Venna, J. B. Jasinski and M. A. Carreon, J. Am. Chem. Soc 132 (51), 18030-18033 (2010).
- B. Wang, A. P. Cote, H. Furukawa, M. O'Keeffe and O. M. Yaghi, Nature 453 (7192), 207-U206 (2008).
- 6. Q. L. Song, S. K. Nataraj, M. V. Roussenova, J. C. Tan, D. J. Hughes, W. Li, P. Bourgoin, M. A. Alam, A. K. Cheetham, S. A. Al-Muhtaseb and E. Sivaniah, Energy Environ. Sci **5** (8), 8359-8369 (2012).
- 7. S. Japip, H. Wang, Y. C. Xiao and T. S. Chung, J. Membr. Sci **467**, 162-174 (2014).

- 8. F. Cacho-Bailo, G. Caro, M. Etxeberria-Benavides, O. Karvan, C. Tellez and J. Coronas, ChemComm **51** (56), 11283-11285 (2015).
- 9. Y. Hu, Z. X. Liu, J. Xu, Y. N. Huang and Y. Song, J. Am. Chem. Soc **135** (25), 9287-9290 (2013).
- 10. G. Lu and J. T. Hupp, J. Am. Chem. Soc 132 (23), 7832-+ (2010).
- 11. W. Meng, Y. Y. Wen, L. Dai, Z. X. He and L. Wang, Sens. Actuators B Chem. **260**, 852-860 (2018).
- 12. C. H. Kuo, Y. Tang, L. Y. Chou, B. T. Sneed, C. N. Brodsky, Z. P. Zhao and C. K. Tsung, J. Am. Chem. Soc **134** (35), 14345-14348 (2012).
- 13. L. T. L. Nguyen, K. K. A. Le, H. X. Truong and N. T. S. Phan, Catal. Sci. Technol. 2 (3), 521-528 (2012).
- 14. J. Zakzeski, A. Debczak, P. C. A. Bruijnincx and B. M. Weckhuysen, Appl. Catal. A-Gen **394** (1-2), 79-85 (2011).
- 15. H. Yang, X. W. He, F. Wang, Y. Kang and J. Zhang, J. Mater. Chem **22** (41), 21849-21851 (2012).
- 16. J. N. Qin, S. B. Wang and X. C. Wang, Appl. Catal. B-Environ. 209, 476-482 (2017).
- 17. B. Pattengale, S. Z. Yang, S. Lee and J. Huang, ACS Catal. 7 (12), 8446-8453 (2017).
- 18. S. W. Liu, F. Chen, S. T. Li, X. X. Peng and Y. Xiong, Appl. Catal. B-Environ. **211**, 1-10 (2017).
- 19. M. Wang, J. X. Liu, C. M. Guo, X. S. Gao, C. H. Gong, Y. Wang, B. Liu, X. X. Li, G. G. Gurzadyan and L. C. Sun, J. Mater. Chem. A 6 (11), 4768-4775 (2018).
- 20. W. M. Zhang, X. Y. Yao, S. N. Zhou, X. W. Li, L. Li, Z. Yu and L. Gu, Small 14 (24) (2018).
- 21. N. N. Du, C. M. Wang, R. Long and Y. J. Xiong, Nano Res. **10** (9), 3228-3237 (2017).
- S. B. Wang, B. Y. Guan, X. Wang and X. W. D. Lou, J. Am. Chem. Soc 140 (45), 15145-15148 (2018).
- 23. X. Wang, L. Yu, B. Y. Guan, S. Y. Song and X. W. Lou, Adv. Mater. 30 (29) (2018).
- 24. A. Aijaz, J. Masa, C. Rosler, W. Xia, P. Weide, A. J. R. Botz, R. A. Fischer, W. Schuhmann and M. Muhler, Angew. Chem. Int. Ed. **55** (12), 4087-4091 (2016).
- 25. B. Pattengale, S. Z. Yang, J. Ludwig, Z. Q. Huang, X. Y. Zhang and J. Huang, J. Am. Chem. Soc **138** (26), 8072-8075 (2016).
- 26. B. Pattengale, D. J. SantaLucia, S. Z. Yang, W. H. Hu, C. M. Liu, X. Y. Zhang, J. F. Berry and J. Huang, J. Am. Chem. Soc **140** (37), 11573-11576 (2018).
- 27. B. Pattengale and J. Huang, Phys. Chem. Chem. Phys **20** (21), 14884-14888 (2018).
- 28. H. Kato and K. Akimoto, J. Am. Chem. Soc 96 (5), 1351-1357 (1974).
- 29. S. Z. Yang, B. Pattengale, E. L. Kovrigin and J. Huang, ACS Energy Lett. 2 (1), 75-80 (2017).
- 30. Y. X. Zhou, W. H. Hu, S. Z. Yang and J. Huang, Phys. Chem. Chem. Phys **22** (7), 3849-3854 (2020).
- 31. R. S. Swathi and K. L. Sebastian, J. Chem. Sci 121 (5), 777-787 (2009).
- 32. R. Narayanan, M. Deepa and A. K. Srivastava, J. Mater. Chem. A **1** (12), 3907-3918 (2013).
- 33. H. T. Zhou, C. B. Qin, R. Y. Chen, W. J. Zhou, G. F. Zhang, Y. Gao, L. T. Xiao and S. T. Jia, J. Phys. Chem. Lett. **10** (11), 2849-2856 (2019).
- 34. R. E. Dale and J. Eisinger, Biopolymers 13 (8), 1573-1605 (1974).
- 35. B. Albinsson, M. P. Eng, K. Pettersson and M. U. Winters, Phys. Chem. Chem. Phys **9** (44), 5847-5864 (2007).
- 36. C. R. Sabanayagam, J. S. Eid and A. Meller, J. Chem. Phys. 122 (6) (2005).
- 37. A. A. Deniz, M. Dahan, J. R. Grunwell, T. J. Ha, A. E. Faulhaber, D. S. Chemla, S. Weiss and P. G. Schultz, Proc. Natl. Acad. Sci. U.S.A **96** (7), 3670-3675 (1999).
- 38. R. B. Sekar and A. Periasamy, J. Cell Biol. 160 (5), 629-633 (2003).
- 39. F. Federspiel, G. Froehlicher, M. Nasilowski, S. Pedetti, A. Mahmood, B. Doudin, S. Park, J. O. Lee, D. Halley, B. Dubertret, P. Gilliot and S. Berciaud, Nano Lett. **15** (2), 1252-1258 (2015).
- 40. R. S. Swathi and K. L. Sebastian, J. Chem. Phys. **130** (8) (2009).
- 41. T. Park, H. Kim, M. Leem, W. Ahn, S. Choi, J. Kim, J. Uh, K. Kwon, S. J. Jeong, S. Park, Y. Kim and H. Kim, RSC Adv. **7** (2), 884-889 (2017).
- 42. V. Vandalon and W. Kessels, Langmuir **35** (32), 10374-10382 (2019).
- 43. O. M. E. Ylivaara, X. W. Liu, L. Kilpi, J. Lyytinen, D. Schneider, M. Laitinen, J. Julin, S.
- Ali, S. Sintonen, M. Berdova, E. Haimi, T. Sajavaara, H. Ronkainen, H. Lipsanen, J. Koskinen, S. P. Hannula and R. L. Puurunen, Thin Solid Films **552**, 124-135 (2014).
- 44. J. Kallioinen, G. Benko, V. Sundstrom, J. E. I. Korppi-Tommola and A. P. Yartsev, J. Phys. Chem. B **106** (17), 4396-4404 (2002).
- 45. N. H. Damrauer, G. Cerullo, A. Yeh, T. R. Boussie, C. V. Shank and J. K. McCusker, Science **275** (5296), 54-57 (1997).
- J. B. Asbury, R. J. Ellingson, H. N. Ghosh, S. Ferrere, A. J. Nozik and T. Q. Lian, J. Phys. Chem. B 103 (16), 3110-3119 (1999).
 O. Flender, M. Scholz, J. R. Klein, K. Oum and T. Lenzer, Phys. Chem. Chem. Phys 18
- (37), 26010-26019 (2016). 48. M. Fakis, P. Hrobarik, O. Yushchenko, I. Sigmundova, M. Koch, A. Rosspeintner, E.
- M. Fakis, F. Hiddarik, C. Hashchenko, I. Sgirlanduda, M. Roch, A. Rosspendier, E. Stathatos and E. Vauthey, J. Phys. Chem. C 118 (49), 28509-28519 (2014).
 M. Rehorek, N. A. Dencher and M. P. Heyn, Biochemistry 24 (21), 5980-5988 (1985).
- 50. G. Ramos-Ortiz, Y. Oki, B. Domercq and B. Kippelen, Phys. Chem. Chem. Phys **4** (17), 4109-4114 (2002).
- 51. B. R. Lee, W. Lee, T. L. Nguyen, J. S. Park, J. S. Kim, J. Y. Kim, H. Y. Woo and M. H. Song, ACS Appl. Mater. Interfaces **5** (12), 5690-5695 (2013).
- 52. X. Zhang, C. A. Marocico, M. Lunz, V. A. Gerard, Y. K. Gun'ko, V. Lesnyak, N. Gaponik, A. S. Susha, A. L. Rogach and A. L. Bradley, ACS Nano **8** (2), 1273-1283 (2014).